IEEE Access
Multidisciplinary | Rapid Review | Open Access Journal

Received August 14, 2020, accepted September 28, 2020, date of publication October 8, 2020, date of current version October 22, 2020.

Digital Object Identifier 10.1109/ACCESS.2020.3029566

FEM and BEM Implementations of a High Order Surface Impedance Boundary Condition for Three-Dimensional Eddy Current Problems

JINLONG DONG[1,2] AND LUCA DI RIENZO[1], (Senior Member, IEEE)
[1]Dipartimento di Elettronica, Informazione e Bioingegneria, Politecnico di Milano, 20133 Milan, Italy
[2]State Key Laboratory of Electrical Insulation and Power Equipment, Xi'an Jiaotong University, Xi'an 710049, China
Corresponding author: Luca Di Rienzo (luca.dirienzo@polimi.it)

ABSTRACT We implement a three-dimensional formulation for eddy current problems based on the reduced magnetic scalar potential enforcing a high order surface impedance boundary condition (SIBC) which takes into account the curvatures of the conductor surface. Based on perturbation theory, the formulation reduces to three Laplace boundary value problems with Neumann boundary conditions and hence can be easily implemented in any existing Finite Element Method (FEM) or Boundary Element Method (BEM) code for the Laplace equation. The appropriate choice of the small parameter in the perturbation approach correctly represents the order of accuracy of the SIBC. The validation is carried out by comparison with full FEM solutions of a canonical test problem and of a more realistic example of a non-destructive testing probe. The validity of the extension of a high order SIBC to lower frequencies is verified and the fields can be obtained at any frequency in the range of interest once the formulation is solved only once.

INDEX TERMS Surface impedance boundary condition, boundary element method, finite element method, eddy currents.

I. INTRODUCTION

Three dimensional eddy current problems characterized by strong skin effect conditions are computationally challenging due to the appearance of a boundary layer phenomenon. The SIBC is a standard and efficient tool for this kind of problems and dates back to the work of Leontovich [1]. It provides approximate relations between electromagnetic quantities at the surface of the conductor, so that the conducting region does not need to be included in the numerical model.

The conditions proposed in [1] only take into account the local tangential plane at each point of the surface, and for this reason they are only valid for very thin skin layers. Rytov proposed, in [2], an extension of Leontovich SIBC based on the principle of an asymptotic expansion of the fields in terms of the skin depth. Extension of the Rytov's approach to general smooth conductors have been introduced independently in [3] (and references therein) and [4] and, moreover, in [4] the mathematics of the related asymptotic expansions are suitably understood.

SIBCs are widely used in commercial softwares in their low order degree of approximation (according to [1]) and many implementations can be found in literature. On the other hand, for eddy current problems there are no implementations of three dimensional BEM or FEM formulations enforcing SIBC of high order of approximation, which allows for surface curvature. In [5] and [3] theoretical formulations are presented, but their implementations are carried out only for 2D examples.

Two dimensional implementations of high order SIBCs in BEM and FEM are described in detail in [6], [7], [9]. In [10] an experimental validation is also provided. An extension to the nonlinear case is proposed in [11].

An implementation of Leontovich SIBC with unstructured-partial element equivalent circuit (PEEC) is described in [12]. Thanks to the circuit representation, the PEEC formulation can be easily and naturally coupled with external circuits. Coupling of low order SIBC with Surface Integral Equation Methods have been proposed for full wave problems, e.g. in [13] and references therein.

In this paper three-dimensional FEM and BEM implementations in terms of the reduced magnetic scalar potential [14] and enforcing a high order SIBC are analysed. Since the proposed formulation is formed by a sequence of Neumann problems for the Laplace equation, its implementation can be carried out with the help of any BEM or FEM code for the Laplace equation. This is the main advantage of the proposed formulation.

The associate editor coordinating the review of this manuscript and approving it for publication was Paolo Bettini.

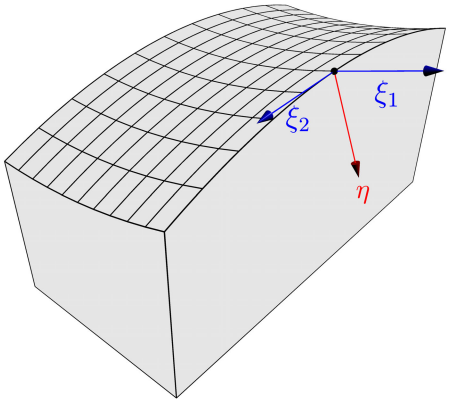

FIGURE 1. Local coordinate system on the surface of the conductive domain.

The accuracy and the conditions of applicability of the formulation are investigated by solving a canonical test case and a more applicative example, with the help of a commercial software. The formulation can be applied only in the case of smooth surfaces. The presence of edges and corners would introduce local errors.

II. PERTURBATIVE FORMULATION

A. THE PERTURBATION APPROACH

As is well known, the diffusion of a time-harmonic magnetic field in a good conductor with magnetic permeability $\mu = \mu_0\mu_r$ is characterized by the skin depth, defined as

$$\delta = \sqrt{\frac{2}{\omega\mu_0\mu_r\sigma}} = \sqrt{\frac{\tau}{\mu_0\mu_r\sigma}}, \quad \tau = \frac{2}{\omega} \tag{1}$$

where ω is the angular frequency and σ the electric conductivity.

We will follow the perturbation approach described in [3]–[5]. We introduce a local orthogonal coordinate system (ξ_1, ξ_2, η) laying on the surface of the conductor (Fig. 1). According to perturbation theory we normalize the physical quantities using scale factors

$$\tilde{t} = \frac{t}{\tau}, \quad \tilde{\xi}_k = \frac{\xi_k}{D}, \quad \tilde{d}_k = \frac{d_k}{D}, \quad \tilde{\eta} = \frac{\eta}{\mu_r\delta} \tag{2}$$

where d_k is the local radius of curvature corresponding to ξ_k, D is a characteristic size of the conductor and τ is a characteristic time, equal to $\frac{2}{\omega}$ in the time-harmonic case. From now on all the non-dimensional quantities are indicated with a tilde. We then define the non-dimensional small parameter as

$$\tilde{p} = \frac{\mu_r\delta}{D} \tag{3}$$

Definition (3) differs from the one used in [3], [5], where $\tilde{p} = \frac{\delta}{D}$. This improvement is crucial for the correct condition of applicability of the formulation in the case of magnetic conductors, as will be shown in Section III.

In the conductive domain the magnetic field $\mathbf{h}$ obeys the diffusion equation, which reads

$$\nabla \times (\nabla \times \mathbf{h}) = -\mu\sigma\frac{\partial \mathbf{h}}{\partial t} = -\frac{\mu\sigma}{\tau}\frac{\partial \mathbf{h}}{\partial \tilde{t}} = -\frac{1}{\delta^2}\frac{\partial \mathbf{h}}{\partial \tilde{t}} \tag{4}$$

We apply the Laplace transform to (4) obtaining

$$\nabla \times (\nabla \times \mathbf{H}) = -\frac{1}{\delta^2}s\mathbf{H} \tag{5}$$

where

$$\mathbf{H}(s) = \int_0^{+\infty} \mathbf{h}(\tilde{t}) \exp(-s\tilde{t}) d\tilde{t} \tag{6}$$

Following [3]–[5] we write (5) in the local coordinate system. We then expand the magnetic field in the power series of $\tilde{p}$

$$\mathbf{H} = \sum_{m=0}^{+\infty} \tilde{p}^m \mathbf{H}_m \tag{7}$$

Introducing expansion (7) into the diffusion equation written in the local coordinate system and equating the terms with equal power of $\tilde{p}$ for $m = 0$ we obtain

$$\frac{\partial^2 (\mathbf{H}_0)_{\tilde{\xi}_k}}{\partial \tilde{\eta}^2} = \mu_r^2 s (\mathbf{H}_0)_{\tilde{\xi}_k} \tag{8a}$$

$$\mu_r^2 s (\mathbf{H}_0)_{\tilde{\eta}} = 0 \tag{8b}$$

where $(\cdot)_{\tilde{\xi}_k}$ and $(\cdot)_{\tilde{\eta}}$ are respectively the $\tilde{\xi}_k$ and $\tilde{\eta}$ components of the fields.

Solutions of (8a)-(8b) are given by

$$(\mathbf{H}_0)_{\tilde{\xi}_k} = \left(\mathbf{H}_0^b\right)_{\tilde{\xi}_k} \exp\left(-\mu_r\sqrt{s}\tilde{\eta}\right) \tag{9a}$$

$$(\mathbf{H}_0)_{\tilde{\eta}} = 0 \tag{9b}$$

where apex b indicates the fields evaluated at the boundary between the conductive and the dielectric media.

Following the same approach, for $m = 1$ we obtain

$$\frac{\partial^2 (\mathbf{H}_1)_{\tilde{\xi}_k}}{\partial \tilde{\eta}^2} - \mu_r s (\mathbf{H}_1)_{\tilde{\xi}_k} = \left(\frac{1}{\tilde{d}_k} + \frac{1}{\tilde{d}_{3-k}}\right)\frac{\partial (\mathbf{H}_0)_{\tilde{\xi}_k}}{\partial \tilde{\eta}} \tag{10a}$$

$$-\mu_r^2 s (\mathbf{H}_1)_{\tilde{\eta}} = \sum_{k=1}^{2} \frac{\partial^2}{\partial \tilde{\xi}_k \partial \tilde{\eta}} (\mathbf{H}_0)_{\tilde{\xi}_k} \tag{10b}$$

whose solutions are given by

$$(\mathbf{H}_1)_{\tilde{\xi}_k} = \left[\left(\mathbf{H}_1^b\right)_{\tilde{\xi}_k} + \tilde{\eta}\frac{(\mathbf{H}_0)_{\tilde{\xi}_k}}{2}\left(\frac{1}{\tilde{d}_k} + \frac{1}{\tilde{d}_{3-k}}\right)\right] \times \exp\left(-\mu_r\tilde{\eta}\sqrt{s}\right) \tag{11a}$$

$$(\mathbf{H}_1)_{\tilde{\eta}} = \frac{1}{\mu_r\sqrt{s}}\sum_{k=1}^{2}\frac{\partial}{\partial \tilde{\xi}_k}\left(\left(\mathbf{H}_0^b\right)_{\tilde{\xi}_k} \exp\left(-\mu_r\sqrt{s}\tilde{\eta}\right)\right) \tag{11b}$$

Finaly for $m = 2$ we have

$$(\mathbf{H}_2)_{\tilde{\eta}} = -\frac{1}{\mu_r^2 s}\sum_{k=1}^{2}\frac{\partial}{\partial \tilde{\xi}_k} \times \left[\frac{\partial (\mathbf{H}_1)_{\tilde{\xi}_k}}{\partial \tilde{\eta}} + \frac{\tilde{\eta}}{\tilde{d}_k}\frac{\partial (\mathbf{H}_0)_{\tilde{\xi}_k}}{\partial \tilde{\eta}} - \frac{(\mathbf{H}_0)_{\tilde{\xi}_k}}{\tilde{d}_k}\right] \tag{12}$$

whose solution is given by

$$(\mathbf{H}_2)_{\tilde{\eta}} = \frac{1}{\mu_r\sqrt{s}}\sum_{k=1}^{2}\frac{\partial}{\partial\tilde{\xi}_k}\left[\left(\mathbf{H}_1^b\right)_{\tilde{\xi}_k} + \tilde{\eta}\frac{\tilde{d}_k+3\tilde{d}_{3-k}}{2\tilde{d}_k\tilde{d}_{3-k}}\left(\mathbf{H}_0^b\right)_{\tilde{\xi}_k} - \frac{1}{\mu_r\sqrt{s}}\frac{\tilde{d}_k-\tilde{d}_{3-k}}{2\tilde{d}_k\tilde{d}_{3-k}}\left(\mathbf{H}_0^b\right)_{\tilde{\xi}_k}\right]\exp\left(-\mu_r\tilde{\eta}\sqrt{s}\right) \tag{13}$$

To switch to the frequency domain it is sufficient to substitute $2j$ to s in the previous formulas.

B. REDUCED MAGNETIC SCALAR POTENTIAL FORMULATION

We want to compute the magnetic field in a dielectric region with $\mu_r = 1$ outside a conductor of volume Ω, with conductivity σ and magnetic permeability $\mu_r\mu_0$, when an external magnetic field is imposed. Following [14] and [5] we represent the magnetic field $\mathbf{H}^{ext}$ in the dielectric space by means of the reduced magnetic scalar potential, as follows

$$\mathbf{H}^{ext} = \mathbf{H}_s - \nabla\phi \tag{14}$$

where $\mathbf{H}_s$ is the imposed external magnetic field. Substituting (14) into $\nabla\cdot\mathbf{H}^{ext} = 0$, we see that the magnetic scalar potential obeys Laplace equation

$$\nabla^2\phi = 0 \tag{15}$$

We adopt an asymptotic expansion in the same form of (7) for the magnetic scalar potential

$$\phi = \sum_{m=0}^{+\infty}\tilde{p}^m\phi_m \tag{16}$$

The boundary conditions at the interface between conductive and dielectric region (characterized by $\mu = \mu_0$) require that

$$\left(\mathbf{H}_0^b\right)_{\tilde{\xi}_k} + \tilde{p}\left(\mathbf{H}_1^b\right)_{\tilde{\xi}_k} + \tilde{p}^2\left(\mathbf{H}_2^b\right)_{\tilde{\xi}_k} = \left[\mathbf{H}_s - \tilde{\nabla}\phi_0 - \tilde{p}\tilde{\nabla}\phi_1 - \tilde{p}^2\tilde{\nabla}\phi_2\right]_{\tilde{\xi}_k}^b \tag{17a}$$

$$\mu_r\left[\left(\mathbf{H}_0^b\right)_{\tilde{\eta}} + \tilde{p}\left(\mathbf{H}_1^b\right)_{\tilde{\eta}} + \tilde{p}^2\left(\mathbf{H}_2^b\right)_{\tilde{\eta}}\right] = \left[\mathbf{H}_s - \tilde{\nabla}\phi_0 - \tilde{p}\tilde{\nabla}\phi_1 - \tilde{p}^2\tilde{\nabla}\phi_2\right]_{\tilde{\eta}}^b \tag{17b}$$

From (17a)-(17b), equating the terms with equal power of $\tilde{p}$ we obtain

$$\left(\mathbf{H}_0^b\right)_{\tilde{\xi}_k} = \left(\mathbf{H}_s - \tilde{\nabla}\phi_0\right)_{\tilde{\xi}_k}^b \tag{18}$$

$$\left(\mathbf{H}_1^b\right)_{\tilde{\xi}_k} = -\left(\tilde{\nabla}\phi_1\right)_{\tilde{\xi}_k}^b \tag{19}$$

$$\left(\mathbf{H}_2^b\right)_{\tilde{\xi}_k} = -\left(\tilde{\nabla}\phi_2\right)_{\tilde{\xi}_k}^b \tag{20}$$

$$\mu_r\left(\mathbf{H}_0^b\right)_{\tilde{\eta}} = \left(\mathbf{H}_s - \tilde{\nabla}\phi_0\right)_{\tilde{\eta}}^b \tag{21}$$

$$\mu_r\left(\mathbf{H}_1^b\right)_{\tilde{\eta}} = -\left(\tilde{\nabla}\phi_1\right)_{\tilde{\eta}}^b \tag{22}$$

$$\mu_r\left(\mathbf{H}_2^b\right)_{\tilde{\eta}} = -\left(\tilde{\nabla}\phi_2\right)_{\tilde{\eta}}^b \tag{23}$$

Using (9b), (15) and (16) the following boundary value problem (BVP) is obtained for $m = 0$

$$\tilde{\nabla}^2\phi_0 = 0 \tag{24a}$$

$$\frac{\partial\phi_0}{\partial\mathbf{n}} = \left(\mathbf{H}_s^b\right)_{\tilde{\eta}} \tag{24b}$$

Evaluating (11b) at $\tilde{\eta} = 0$ we obtain

$$(\mathbf{H}_1)_{\tilde{\eta}=0} = \frac{1}{\mu_r\sqrt{s}}\sum_{k=1}^{2}\frac{\partial}{\partial\tilde{\xi}_k}\left(\mathbf{H}_0^b\right)_{\tilde{\xi}_k} \tag{25}$$

and using (15), (16), and (18) we can write the BVP corresponding to $m = 1$

$$\tilde{\nabla}^2\phi_1 = 0 \tag{26a}$$

$$\frac{\partial\phi_1}{\partial\mathbf{n}} = -\frac{1}{\sqrt{s}}\sum_{k=1}^{2}\frac{\partial}{\partial\tilde{\xi}_k}\left(\mathbf{H}_s - \tilde{\nabla}\phi_0\right)_{\tilde{\xi}_k}^b \tag{26b}$$

In the same way evaluating (13) at $\tilde{\eta} = 0$ we obtain the BVP corresponding to $m = 2$

$$\tilde{\nabla}^2\phi_2 = 0 \tag{27a}$$

$$\frac{\partial\phi_2}{\partial\mathbf{n}} = -\frac{1}{\sqrt{s}}\sum_{k=1}^{2}\frac{\partial}{\partial\tilde{\xi}_k}\left(-\tilde{\nabla}\phi_1\right)_{\tilde{\xi}_k}^b - \frac{1}{\mu_r\sqrt{s}}\frac{\tilde{d}_k-\tilde{d}_{3-k}}{2\tilde{d}_k\tilde{d}_{3-k}}\left(\mathbf{H}_s - \tilde{\nabla}\phi_0\right)_{\tilde{\xi}_k}^b \tag{27b}$$

C. THE BOUNDARY VALUE PROBLEMS

As a first step, BVP (24a) - (24b) must be solved. Being the boundary condition (24b) of Neumann type, the solution ϕ_0 is defined up to an additive constant and in order to ensure its uniqueness its value at infinity is set equal to zero.

Once ϕ_0 is computed over the surface of the conductor, BVP (26a) - (26b) has to be solved, and after it also BVP (27a) - (27b), still setting ϕ_1 and ϕ_2 to zero at infinity

According to (16) the complete solution for ϕ is given by

$$\phi = \phi_0 + \tilde{p}\phi_1 + \tilde{p}^2\phi_2 \tag{28}$$

and the magnetic field in the dielectric space can be computed by means of (14). Keeping only the first term ϕ_0 in the right-hand-side of (28) corresponds to the perfect electric conductor (PEC) approximation. Adding the second term $\tilde{p}\phi_1$ corresponds to Leontovich correction and finally adding $\tilde{p}^2\phi_2$ gives the more accurate Mitzner approximation [3]. In order to summarize the implementation of the formulation, this is described as a pseudocode (Algorithm 1).

A first advantage of the described perturbation approach is that it guarantees that if the third term in (28) is numerically below the threshold of the desidered accuracy, then SIBC of low order can be safely applied. A second advantage is that if the magnetic field is to be computed at different frequencies, the formulation must be solved only once and then the field is obtained at any frequency of interest by means of (28) and (14).

Algorithm 1: FEM or BEM Implementation of the Formulation

Calculate $\mathbf{H}_s$ via Biot-Savart's law from filamentary currents;
Solve BVP (24a) - (24b) using FEM or BEM;
Compute $\mathbf{H}^{ext}_{PEC}$ from ϕ_0 using (14);
Solve BVP (26a) - (26b) using FEM or BEM;
Compute $\phi_{Leontovich} = \phi_0 + \tilde{p}\phi_1$;
Compute $\mathbf{H}^{ext}_{Leontovich}$ from $\phi_{Leontovich}$ using (14);
Solve BVP (27a) - (27b) using FEM or BEM;
Compute $\phi_{Mitzner} = \phi_0 + \tilde{p}\phi_1 + \tilde{p}^2\phi_2$;
Compute $\mathbf{H}^{ext}_{Mitzner}$ from $\phi_{Mitzner}$ using (14);

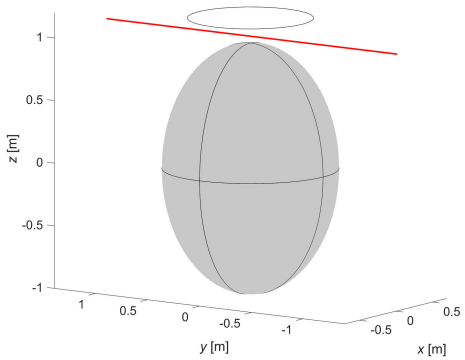

FIGURE 2. Geometry of the test case.

III. NUMERICAL VALIDATION OF FEM AND BEM IMPLEMENTATIONS

In order to validate the formulation and investigate the accuracy of the SIBC approximation, a conductive ($\sigma = 5.998 \cdot 10^7$ S/m) prolate ellipsoid with different principal curvatures (Fig. 2) is considered as a test case. A time-harmonic current of 10 A flows in a circular coil and the z-component of the magnetic field is computed over an horizontal line between the coil and the conductive body. Geometrical dimensions of the test case are summarized in Table 1. All the simulations in the paper are run on a PC Inter(R) Core(TM) i7-10510U CPU @1.8GHz with 16 GB memory. Surface derivatives are implemented with the formulas derived in Appendix. Many methods exist for the estimation of the curvature of surfaces represented by triangular meshes and in [15] a systematic review can be found. Here the values of the surface curvatures are provided by the used commercial software [16].

A. BEM IMPLEMENTATION

The previous formulation is solved using a Galerkin implementation of the BEM available in commercial software [16]. Second order 3162 triangular boundary elements are used. A reference standard FEM solution with a very fine mesh is computed solving an axisymmetric model with the same commercial software.

For all the cases discussed in the following, BVP (24a)-(24b) (PEC approximation) is solved in 60 s using 4.28 GB; BVP (26a)-(26b) (Leontovich approximation) in 133 s using 4.81 GB; finally BVP (27a)-(27b) (Mitzner approximation) in 152 s using 4.73 GB.

TABLE 1. Geometrical dimensions of the test case.

Dimension	[m]
semi-major axis	1
semi-minor axis	0.7
coil radius	0.5
origin-coil center	1.2
Scale factor D	0.5
Line x-coordinate	0.02
Line y-coordinate	$-1.4 < y < 1.4$
Line z-coordinate	1.05

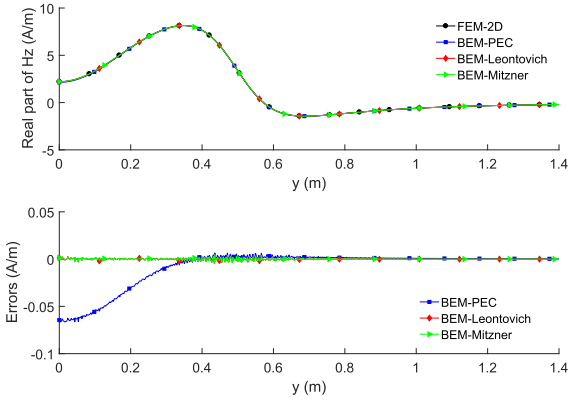

FIGURE 3. Real part of the magnetic field @ 1 kHz ($\mu_r = 1$, $\delta = 2.055$ mm, $\tilde{p} = 4.110 \cdot 10^{-3}$) and corresponding errors.

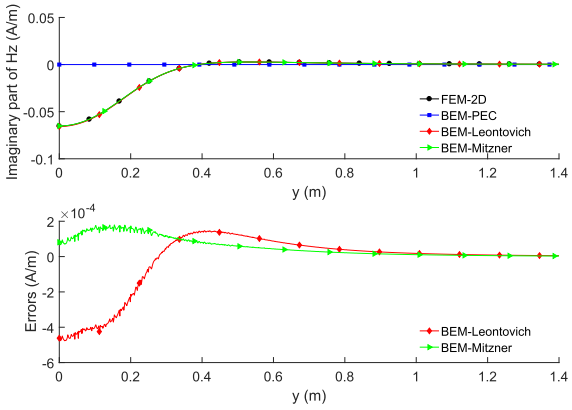

FIGURE 4. Imaginary part of the magnetic field @ 1 kHz ($\mu_r = 1$, $\delta = 2.055$ mm, $\tilde{p} = 4.110 \cdot 10^{-3}$) and corresponding errors.

Let us first consider the case when $\mu_r = 1$. As can be seen in Fig. 3 - 4, when frequency is 1 kHz ($\delta = 2.055$ mm, $\tilde{p} = 4.110 \cdot 10^{-3}$) we are in strong skin effect conditions and in fact the application of Leontovich correction is enough to reach a good accuracy.

Decreasing frequency to 50 Hz ($\delta = 9.190$ mm, $\tilde{p} = 1.838 \cdot 10^{-2}$) justifies the use of Mitzner correction (Fig. 5 - 6). Since the current flowing in the coil is real, Mitzner correction only changes the imaginary component of the magnetic field, as can be observed from (27a)-(27b).

In cases when the conductive domain is characterized by $\mu_r > 1$, even if skin depth (1) is small, Mitzner correction

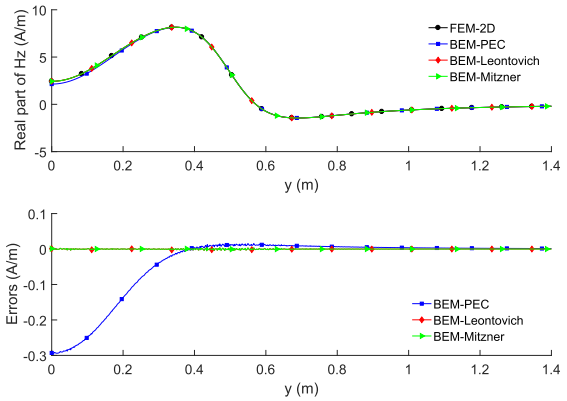

FIGURE 5. Real part of the magnetic field @ 50 Hz ($\mu_r = 1$, $\delta = 9.190$ mm, $\tilde{p} = 1.838 \cdot 10^{-2}$) and corresponding errors.

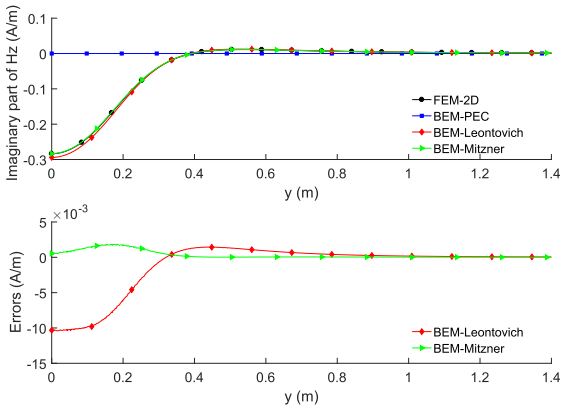

FIGURE 6. Imaginary part of the magnetic field @ 50 Hz ($\mu_r = 1$, $\delta = 9.190$ mm, $\tilde{p} = 1.838 \cdot 10^{-2}$) and corresponding errors.

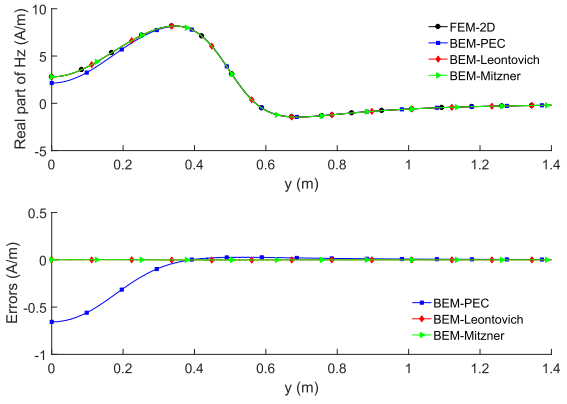

FIGURE 7. Real part of the magnetic field @ 1 kHz ($\mu_r = 100$, $\delta = 0.2055$ mm, $\tilde{p} = 4.110 \cdot 10^{-2}$) and corresponding errors.

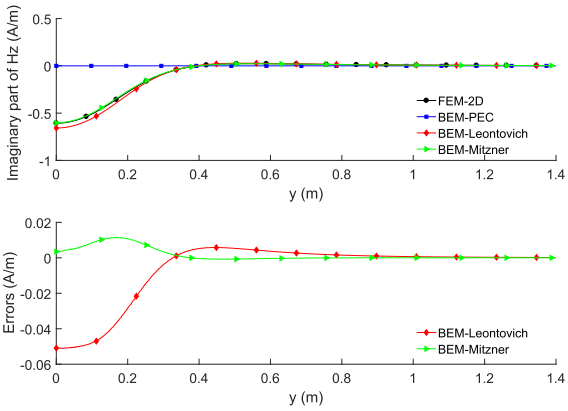

FIGURE 8. Imaginary part of the magnetic field @ 1 kHz ($\mu_r = 100$, $\delta = 0.2055$ mm, $\tilde{p} = 4.110 \cdot 10^{-2}$) and corresponding errors.

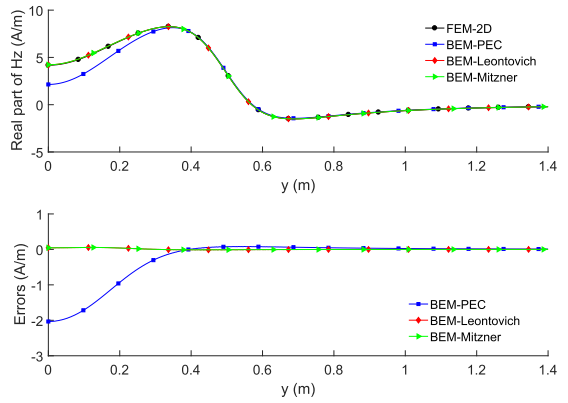

FIGURE 9. Real part of the magnetic field for @ 1 kHz ($\mu_r = 1000$, $\delta = 0.064986$ mm, $\tilde{p} = 1.298 \cdot 10^{-1}$) and corresponding errors.

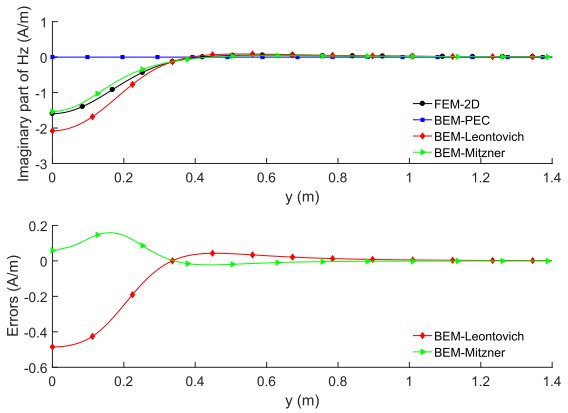

FIGURE 10. Imaginary part of the magnetic field @ 1 kHz ($\mu_r = 1000$, $\delta = 0.064986$ mm, $\tilde{p} = 1.298 \cdot 10^{-1}$) and corresponding errors.

may not give results accurate enough. This can be explained with the appropriate definition of the small parameter (3). For example, Fig. 7-8 shows that in the case of $\mu_r = 100$, $\delta = 0.2055$ mm and $\tilde{p} = 4.110 \cdot 10^{-2}$ only Mitzner approximation gives good results, while Fig. 9-10 shows that in the case of $\mu_r = 1000, \delta = 0.064986$ mm, $\tilde{p} = 1.298 \cdot 10^{-1}$ a higher order approximation would be needed.

B. FEM IMPLEMENTATION

The three BVPs are also solved with FEM using the same commercial software [16]. The obtained results are practically coincident with those of the previous BEM implementation. To deal with the unbounded nature in the FEM models, infinite elements are used. Dirichlet boundary condition is imposed on the outer surface of the infinite element domain to ensure a unique solution.

When using a tetrahedral mesh and second order finite elements (1341980 degrees of freedom), the computational times and required memory are the following: 33 s and 5.44 GB for PEC; 52 s and 6.33 GB for Leontovich; 55 s and 6.45 GB for Mitzner. Hence with this FEM discretization

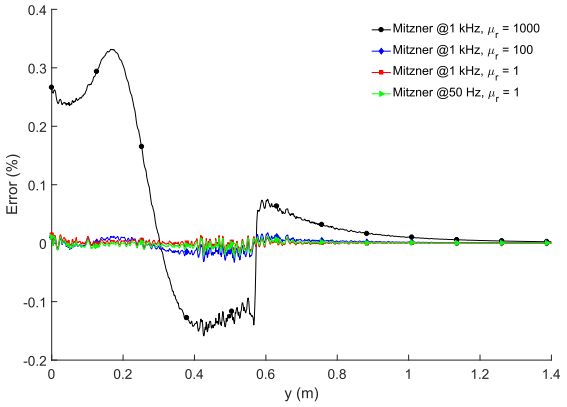

FIGURE 11. Relative error on the rms of the the $z-$ component of the magnetic field with FEM implementation.

the total computational time is shorter than with BEM (2 min, 20 sec).

Fig. 11 summarizes the previous results and is obtained with the FEM implementation. It reports the relative error on the magnitude of the $z-$component of the magnetic field using Mitzner approximation, at different frequencies and at different values of μ_r.

C. COMPUTATION OF THE MAGNETIC FIELD INSIDE THE CONDUCTOR

After the BVPs have been solved, the formulation also gives the possibility to compute the analytical expression of the magnetic field in the boundary layer inside the conductors in a post-processing phase, which may be required in many applications. According to (9b) the normal component of the magnetic field in the PEC approximation is obviously zero, and (11b) and (13) give the Leotovich and Mitzner corrections, respectively.

In Fig. (13)-(14) the normal component of the magnetic field computed according to the above formulas is compared with the 2D FEM solution over the line depicted in Fig. (12) and the good agreement can be noted. Furthermore, in the case of Fig. (14) Mitzner approximation is needed for a good accuracy, as also noted for the same case in the computation of the magnetic field outside the conductor (Fig. (7)-(8)).

IV. APPLICATION TO A NON-DESTRUCTIVE SENSOR SYSTEM

The model of an electromagnetic Helmholtz-coil probe coaxial with a tube as described in [17] is considered (Fig. 15). Each of the two coils (of diameter equal to 140 mm) carries an AC current of 10 A (rms) at frequency $f = 1$ kHz. The distance between the coils is 45 mm. The tube has an outer diameter of 65 mm and an inner diameter of 35 mm and is made of alluminum with conductivity $\sigma = 3.774 \cdot 10^7$ S/m and permeability $\mu_r = 1$. The length of the considered specimen is 400 mm. At the given frequency the skin depth is $\delta = 2.5907$ mm, much lower than the thickness of the tube so that the strong skin effect condition is fulfilled. Here an axial-symmetric model is chosen on purpose in order to have a reference solution given by a 2D axial-symmetric FEM

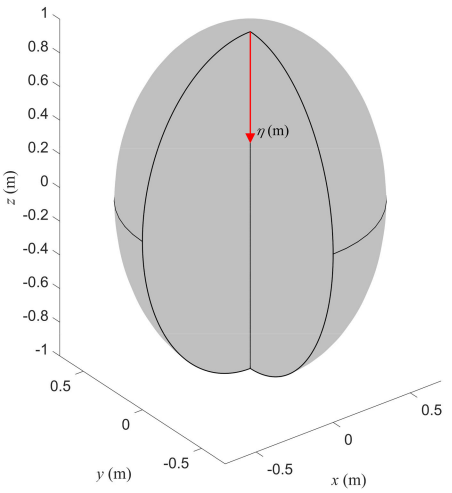

FIGURE 12. Line going into the conductor where the normal component of the magnetic field is computed.

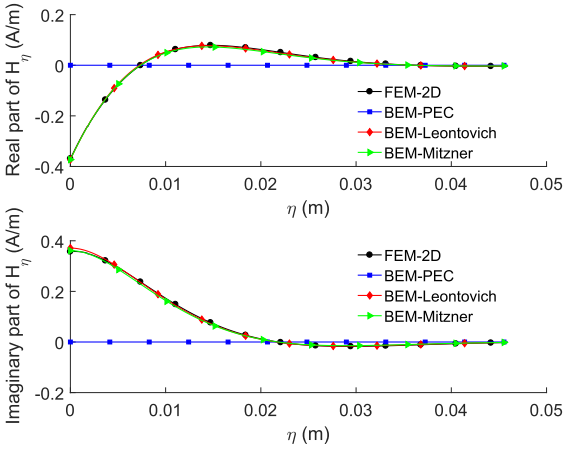

FIGURE 13. Real and imaginary part of the normal component of the magnetic field over line depicted in Fig.(12) @ 50 Hz and $\mu_r = 1$.

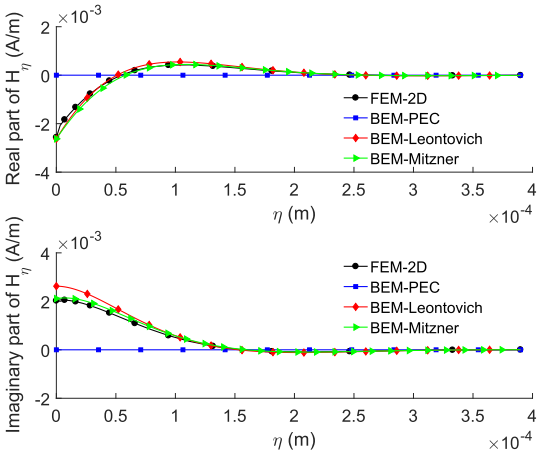

FIGURE 14. Real and imaginary part of the normal component of the magnetic field over line depicted in Fig.(12) @ 1 kHz and $\mu_r = 1000$.

formulation solved with commercial software [16] using a very fine mesh.

The magnetic field over a line (red in the figure) parallel to the tube and at a distance of 3 mm is computed by means of

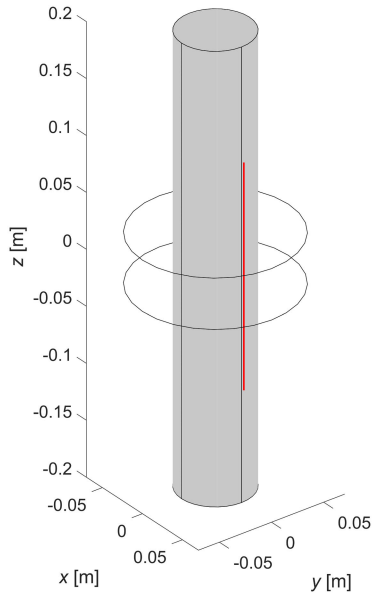

FIGURE 15. Model of the electromagnetic Helmholtz-coil probe.

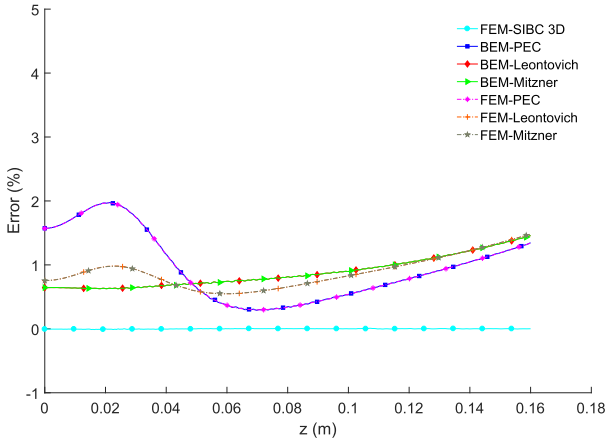

FIGURE 16. Relative error on the rms of the $z-$ component of the magnetic field over half of the red line of Fig. 15 in the case without crack.

the 2D axial-symmetric FEM formulation. As can be noted from Fig. 16, Leontovich and Mitzner approximations give results of the same accuracy.

BEM implementation is carried out with 19492 unknowns. PEC approximation is obtained in 87 s using 4.27 GB of RAM; Leontovich approximation in 158 s with 4.37 GB; Mitzner solution is performed in 178 s using 5 GB.

FEM implementation is carried out with tetrahedral second order nodal finite elements and 1981530 degrees of freedom. PEC approximation is obtained in 65 s using 5.25 GB; Leontovich approximation in 149 s with 11.16 GB; Mitzner solution is performed in 150 s using 11.32 GB.

For this case the SIBC already available in [16] is very accurate, even if at the expenses of a higher computational burden. As a matter of fact it is based on a magnetic vector potential formulation and quadratic edge elements. Using 5487088 degrees-of-freedom the computation takes 1266 s and 11.56 GB.

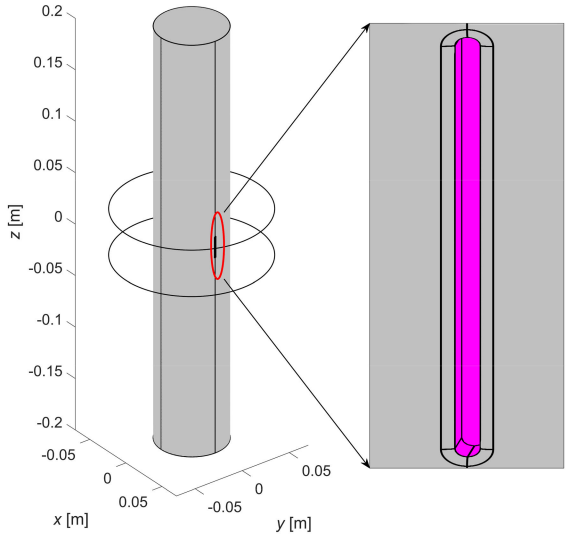

FIGURE 17. Model of the electromagnetic Helmholtz-coil probe and the tube with crack.

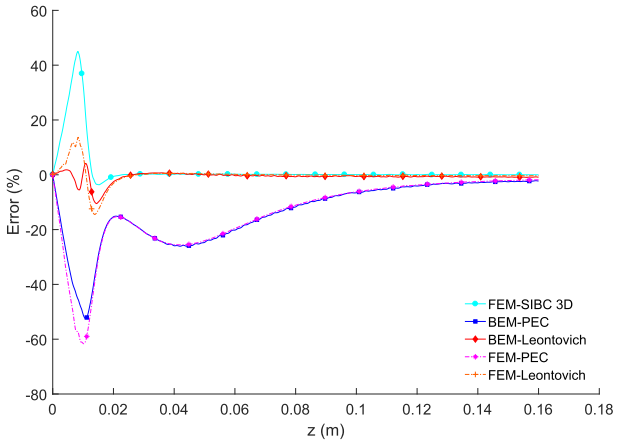

FIGURE 18. Relative error on the rms of the $x-$ component of the magnetic field over half of the red line of Fig. 15 in the case with crack.

The same model of above but with the presence of a crack is then solved with the proposed method (Fig. 17). The crack length (along the z-axis) is 20 mm, its depth is 5 mm and its width (along the y-axis) is 0.8 mm.

In this non-destructive testing technique the detectability of the crack is based on the difference in the magnetic field with respect to the ideal case without any crack. Unfortunately, the presence of the edges of the crack does not allow the application of Mitzner SIBC, which requires the conductor surface to be smooth. Hence only Leontovich SIBC is applied and the results are compared with a reference 3D FEM simulation obtained with [16].

In this case our formulation at a first order (Leontovich) approximation is of the same accuracty of the 3D FEM solution using the SIBC available in [16]. The BVPs with PEC and Leontovich conditions are solved using BEM in 127 s (4.97 GB) and 276 s (5.32 GB) respectively. On the other hand with FEM they are solved with 2385620 degrees-of-freedom in 85 s with 7.93 GB and 269 s with 9.23 GB respectively.

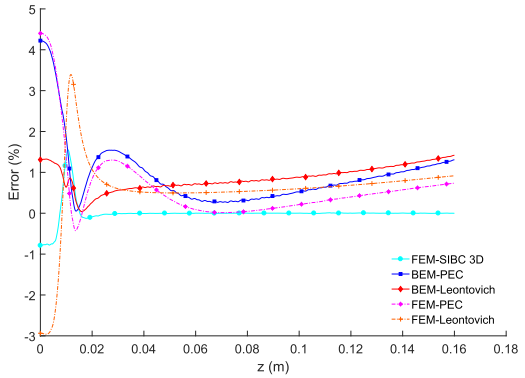

FIGURE 19. Relative error on the rms of the $z-$ component of the magnetic field over half of the red line of Fig. 15 in the case with crack.

The solution of the three dimensional problem using FEM and SIBC with [16] uses 5339418 unknowns, 11.63 GB of RAM and takes 1084 s.

V. CONCLUSION

In the paper FEM and BEM implementations of a three dimensional formulation for eddy current problems enforcing a high order SIBC have been proposed for the first time in three dimensions. The obtained results are compared with a standard FEM solution of a canonical problem and of a more realistic application.

It is so verified that the use of a high order SIBC extends to lower frequencies the range of applicabilty of the surface impedance concept, by taking into account the curvature of the conductive surface.

According to the perturbation approach, it is shown that a good accuracy can be reached only if $\frac{\mu_r \delta}{D} \ll 1$ (being D the characteristic size of the conductive domain), clarifying the condition of applicability in the case of magnetic materials.

The first advantage of the proposed formulation is that it reduces to three scalar Laplace boundary value problems so that any existing FEM or BEM solver for Laplace equation can be used. Based on a scalar potential formulation the approach reveals to be much lighter and faster than a 3D magnetic vector potential FEM formulation enforcing SIBC available in commercial softwares.

A second advantage is that if a frequency domain analysis is needed, the formulation must be solved only once and then the fields are obtained at any frequency in the range of interest and of applicability, a feature not available in any commercial software.

APPENDIX
SURFACE DERIVATIVE OF A VECTOR

Let us consider the global cartesian coordinate system (x, y, z) with unit vectors $\left(\vec{e}_x, \vec{e}_y, \vec{e}_z\right)$ and the local orthogonal coordinate system (ξ_1, ξ_2, η) with unit vectors $\left(\vec{e}_{\xi_1}, \vec{e}_{\xi_2}, \vec{e}_\eta\right)$. Lamè coefficients of the local coordinate system are given by

$$h_{\xi_1} = 1 - c_1\eta, \quad h_{\xi_2} = 1 - c_2\eta, \quad h_\eta = 1 \tag{29}$$

where c_1, c_2 are the principal curvatures of the two coordinate lines corresponding to ξ_1 and ξ_2.

Indicating with $\vec{r} = x\vec{e}_x + y\vec{e}_y + z\vec{e}_z$ the position vector in the global coordinate system, the unit vectors of the local system are given by

$$\vec{e}_{\xi_k} = \frac{\frac{\partial \vec{r}}{\partial \xi_k}}{\left|\frac{\partial \vec{r}}{\partial \xi_k}\right|} = \frac{1}{h_{\xi_k}}\frac{\partial \vec{r}}{\partial \xi_k} \quad k = 1, 2; \; \vec{e}_\eta = \frac{\frac{\partial \vec{r}}{\partial \eta}}{\left|\frac{\partial \vec{r}}{\partial \eta}\right|} = \frac{1}{h_\eta}\frac{\partial \vec{r}}{\partial \eta} \tag{30}$$

In the formulation presented in the paper the derivatives of the surface components of a vector with respect to ξ_k are needed. Given a vector field $\mathbf{V}$ defined on a surface, this can be represented in the global coordinate system as $\mathbf{V} = V_1\vec{e}_x + V_2\vec{e}_y + V_3\vec{e}_z$ and in the local coordinate system as $\mathbf{V} = V_{\xi_1}\vec{e}_{\xi_1} + V_{\xi_2}\vec{e}_{\xi_2} + V_\eta\vec{e}_\eta$. Then

$$\frac{\partial V_{\xi_k}}{\partial \xi_k} = \frac{\partial\left(\mathbf{V}\cdot\vec{e}_{\xi_k}\right)}{\partial \xi_k} = \frac{\partial \mathbf{V}}{\partial \xi_k}\cdot\vec{e}_{\xi_k} + \frac{\partial \vec{e}_{\xi_k}}{\partial \xi_k}\cdot\mathbf{V} \tag{31}$$

In order to compute the first term of the RHS of (31), we observe that

$$\frac{\partial \mathbf{V}}{\partial \xi_k} = \frac{\partial \mathbf{V}}{\partial x}\frac{\partial x}{\partial \xi_k} + \frac{\partial \mathbf{V}}{\partial y}\frac{\partial y}{\partial \xi_k} + \frac{\partial \mathbf{V}}{\partial z}\frac{\partial z}{\partial \xi_k} \tag{32}$$

so that, using the definition of the gradient of a vector and (30), we have

$$\frac{\partial \mathbf{V}}{\partial \xi_k} = (\nabla\mathbf{V})\cdot\frac{\partial \vec{r}}{\partial \xi_k} = (\nabla\mathbf{V})\cdot h_{\xi_k}\vec{e}_{\xi_k} \tag{33}$$

As far as the second term of the right hand side of (31) is concerned, it is convenient to use the following relation holding on the surface [18]:

$$\frac{\partial \vec{e}_{\xi_k}}{\partial \xi_k} = c_k\vec{e}_\eta \tag{34}$$

where c_k is the curvature of the ξ_k coordinate line.

To show how the surface derivatives are computed in the formulation of the paper, we apply previous formulas to the right-hand-side of (10b). From (9a)

$$\sum_{k=1}^{2}\frac{\partial^2}{\partial\tilde{\xi}_k\partial\tilde{\eta}}\left(\mathbf{H}_0\right)_{\tilde{\xi}_k} = \sum_{k=1}^{2}\frac{\partial\left(\mathbf{H}_0^b\right)_{\tilde{\xi}_k}}{\partial\tilde{\xi}_k}\left[\left(-\mu_r\sqrt{s}\right)\exp\left(-\mu_r\sqrt{s}\tilde{\eta}\right)\right] \tag{35}$$

From (31), (33), and (34) it follows that

$$\begin{aligned}\frac{\partial\left(\mathbf{H}_0^b\right)_{\tilde{\xi}_k}}{\partial\tilde{\xi}_k} &= \frac{\partial\mathbf{H}_0^b}{\partial\tilde{\xi}_k}\cdot\vec{e}_{\xi_k} + \frac{\partial\vec{e}_{\xi_k}}{\partial\tilde{\xi}_k}\cdot\mathbf{H}_0^b \\ &= \left(\nabla\mathbf{H}_\mathbf{0}^\mathbf{b}\right)\cdot h_{\xi_k}\vec{e}_{\xi_k} + c_k\vec{e}_\eta\cdot\mathbf{H}_0^b\end{aligned} \tag{36}$$

Finally we have

$$\begin{aligned}&\sum_{k=1}^{2}\frac{\partial^2}{\partial\tilde{\xi}_k\partial\tilde{\eta}}\left(\mathbf{H}_0\right)_{\tilde{\xi}_k} \\ &= \sum_{k=1}^{2}\left[\left(\nabla\mathbf{H}_\mathbf{0}^\mathbf{b}\right)\cdot h_{\xi_k}\vec{e}_{\xi_k} + c_k\vec{e}_\eta\cdot\mathbf{H}_0^b\right]\left(-\mu_r\sqrt{s}\right) \\ &\quad\times\exp\left(-\mu_r\sqrt{s}\tilde{\eta}\right)\end{aligned} \tag{37}$$

REFERENCES

[1] M. A. Leontovich, "On the approximate boundary conditions for the electromagnetic field on the surface of well conducting bodies," *Investigations Radio Waves*, vol. 46, no. 9, pp. 5–12, 1948.
[2] S. M. Rytov, "Calcul du skin-effect par la méthode des perturbations," *J. Phys. USSR*, vol. 2, no. 3, pp. 233–242, 1940.
[3] S. Yuferev and L. Di Rienzo, "Surface impedance boundary conditions in terms of various formalisms," *IEEE Trans. Magn.*, vol. 46, no. 9, pp. 3617–3628, Sep. 2010.
[4] H. Haddar, P. Joly, and H.-M. Nguyen, "Generalized impedance boundary conditions for scattering by strongly absorbing obstacles: The scalar case," *Math. Models Methods Appl. Sci.*, vol. 15, no. 8, pp. 1273–1300, Aug. 2005.
[5] S. Yuferev and N. Ida, *Surface Impedance Boundary Conditions*. Boca Raton, FL, USA: CRC Press, 2010, pp. 143–155.
[6] S. Barmada, L. Di Rienzo, N. Ida, and S. Yuferev, "Time domain surface impedance concept for low frequency electromagnetic problems—Part II: Application to transient skin and proximity effect problems in cylindrical conductors," *IEE Proc.-Sci., Meas. Technol.*, vol. 152, no. 5, pp. 207–216, 2005.
[7] R. Vázquez, A. Buffa, and L. Di Rienzo, "NURBS-based BEM implementation of high-order surface impedance boundary conditions," *IEEE Trans. Magn.*, vol. 48, no. 12, pp. 4757–4766, Dec. 2012.
[8] R. Vázquez, A. Buffa, and L. Di Rienzo, "Isogeometric FEM implementation of high-order surface impedance boundary conditions," *IEEE Trans. Magn.*, vol. 50, no. 6, Jun. 2014, Art. no. 7400508.
[9] L. Di Rienzo, S. Yuferev, and N. Ida, "Computation of the impedance matrix of multiconductor transmission lines using high-order surface impedance boundary conditions," *IEEE Trans. Electromagn. Compat.*, vol. 50, no. 4, pp. 974–984, Nov. 2008.
[10] S. Barmada, L. Di Rienzo, N. Ida, and S. Yuferev, "The use of the surface impedance boundary condition in time domain problems: numerical and experimental validation," *Appl. Comput. Electromagn. Soc. J.*, vol. 19, no. 2, pp. 76–83, Jul. 2004.
[11] C. de Falco, L. Di Rienzo, N. Ida, and S. Yuferev, "Nonlinear impedance boundary condition for 2D BEM," *COMPEL-Int. J. Comput. Math. Electr. Electron. Eng.*, vol. 37, no. 2, pp. 772–783, Mar. 2018.
[12] G. Meunier, Q. A. Phan, O. Chadebec, J. M. Guichon, B. Bannwarth, and R. Torchio, "Unstructured PEEC method with the use of surface impedance boundary condition," *COMPEL-Int. J. Comput. Math. Elect. Electron. Eng.*, to be published, doi: 10.1108/COMPEL-01-2020-0023.
[13] Q. Wu, "Characteristic mode analysis of composite metallic–dielectric structures using impedance boundary condition," *IEEE Trans. Antennas Propag.*, vol. 67, no. 12, pp. 7415–7424, Dec. 2019.
[14] I. Mayergoyz, "A new approach to the calculation of three-dimensional skin effect problems," *IEEE Trans. Magn.*, vol. 19, no. 5, pp. 2198–2200, Sep. 1983.
[15] T. D. Gatzke and C. M. Grimm, "Estimating curvature on triangular meshes," *Int. J. Shape Model.*, vol. 12, no. 01, pp. 1–28, Jun. 2006.
[16] *COMSOL Multiphysics Reference Manual, Version 5.3a*, COMSOL AB, Stockholm, Sweden, 2017, pp. 914–924. [Online]. Available: https://www.comsol.com
[17] W. Li, J. Ge, Y. Wu, X. Yin, G. Chen, X. Yuan, J. Liu, and W. Yang, "An electromagnetic Helmholtz-coil probe for arbitrary orientation crack detection on the surface of pipeline," *Mater. Trans.*, vol. 58, no. 4, pp. 641–645, 2017.
[18] P. M. Morse and H. Feshbach, *Methods of Theoretical Physics, Part I*. New York, NY, USA: McGraw-Hill, 1953, p. 26.

JINLONG DONG received the B.S. and M.S. degrees in electrical engineering from Xi'an Jiaotong University, Xi'an, China, in 2012 and 2014, respectively, and the double Ph.D. degree in electrical engineering from Xi'an Jiaotong University and the Politecnico di Milano. His research interests include low-frequency computational electromagnetics, experimental diagnostics of electric arc plasma in circuit breakers, and electromagnetic inverse problems.

LUCA DI RIENZO (Senior Member, IEEE) received the Laurea (M.Sc.) *(cum laude)* and Ph.D. degrees in electrical engineering from the Politecnico di Milano, in 1996 and 2001, respectively, and the B.S. degree *(cum laude)* in mathematics from the Università Statale di Milano, in 2020. He is currently an Associate Professor with the Dipartimento di Elettronica, Informazione e Bioingegneria, Politecnico di Milano. His research interests are in the field of computational electromagnetics and include magnetic inverse problems, integral equation methods, surface impedance boundary conditions, and uncertainty quantification. He is also a member of the Editorial Board of *COMPEL - The International Journal for Computation and Mathematics in Electrical and Electronic Engineering* and *Sensing and Imaging* and an Associate Editor-in-Chief of *The Applied Computational Electromagnetics Society* journal.